Continental Shelf Research 138 (2017) 120–131

Contents lists available at ScienceDirect

Continental Shelf Research

journal homepage: www.elsevier.com/locate/csr

Thermohaline forcing and interannual variability of northwestern inflows into the northern North Sea

Peter M.F. Sheehan[a,*], Barbara Berx[b], Alejandro Gallego[b], Rob A. Hall[a], Karen J. Heywood[a], Sarah L. Hughes[b]

[a] Centre for Ocean and Atmospheric Sciences, School of Environmental Sciences, University of East Anglia, Norwich Research Park, Norwich NR4 7TJ, United Kingdom
[b] Marine Scotland Science, 375 Victoria Road, Aberdeen AB11 9DB, United Kingdom

ARTICLE INFO

Keywords:
North Sea
Fair Isle Current
East Shetland Atlantic Inflow
Thermohaline circulation
Seasonal variability
Interannual variability

ABSTRACT

A long-established, 127 km-long hydrographic section in the northern North Sea at 59.28°N that runs from the eastern coast of Orkney (2.23°W) to the central North Sea (0°) crosses the path of the main inflows of Atlantic water. Data from 122 occupations between 1989 and 2015 are examined to determine the annual cycle and long-term trends of temperature, salinity and depth-varying geostrophic flow across the section. In an average year, the geostrophic flow referenced to the seafloor is at its narrowest (40 km) in winter, during which time it is driven by the strong horizontal salinity gradient; the horizontal temperature gradient is very weak. Velocity exceeds 4 cm s^{-1}, but transport is at a minimum (0.11 Sv). In the deeper water in the east of the section, thermal stratification develops throughout summer and persists until October, whereas the west is tidally mixed all year. The bottom temperature gradient becomes the primary driver of the geostrophic flow, which is fastest (9 cm s^{-1}) in September and broadest (100 km) in October. Maximum transport (0.36 Sv) occurs in October. Throughout the summer, the horizontal salinity gradient weakens, as does its contribution to the flow. However, it nevertheless acts to broaden the flow west of the location of the strongest horizontal temperature gradient. Section-mean de-seasoned temperature is found to be positively correlated to the Atlantic Multidecadal Oscillation and negatively correlated to the North Atlantic Oscillation. These results refine our understanding of the thermohaline forcing of Atlantic inflow into the northern North Sea, particularly in relation to the salinity distribution. Understanding the variability of this inflow is important for understanding the dynamics of the North Sea ecosystem.

1. Introduction

The North Sea is a shallow shelf sea on the northwestern European continental shelf that lies between the United Kingdom and continental Europe (Fig. 1). Inflow to the North Sea from the North Atlantic occurs through the English Channel (English Channel Inflow), between the Orkney and Shetland Islands (Fair Isle Current, FIC), along the eastern coast of the Shetland Islands (East Shetland Atlantic Inflow, ESAI), and along the western slope of the Norwegian Trench (Norwegian Trench Inflow) (Otto et al., 1990; Svendsen et al., 1991; Turrell et al., 1996). Outflow occurs primarily in the Norwegian Coastal Current (NCC) (Damm et al., 1994). The approximate locations of these flows are illustrated in Fig. 1. These currents are, in turn, largely fed by the Shelf-Edge Current, which flows northwards along the European continental margin (Turrell et al., 1996; Marsh et al., 2017). Input to the FIC also occurs from the Scottish Coastal Current, a northward flow along the western coast of Scotland. The Channel Inflow is weak compared with the northern inflows (Otto et al., 1990; Winther and Johannessen, 2006). The Norwegian Trench Inflow is the largest by volume transport (Otto et al., 1990; Winther and Johannessen, 2006) but it retroflects within the Norwegian Trench and flows out with the NCC. Consequently, it is the FIC and ESAI, the northwestern inflows, that have the greatest effect on conditions in the northern North Sea. The waters of the northwestern inflows approximately follow the 100 m isobath southwards down the eastern coast of Scotland before turning eastwards between 57.5 and 58°N and flowing towards Norway. Within the North Sea, the circulation is broadly cyclonic (Otto et al., 1990; Hill et al., 2008).

The rate of oceanic inflow strongly influences the region's ecosystem (Lindley et al., 1990; Holliday and Reid, 2001; Edwards et al., 2002; Beaugrand, 2004), and the FIC and ESAI provide pathways for perturbations of oceanic origin to propagate into the North Sea

* Corresponding author.
E-mail address: p.sheehan@uea.ac.uk (P.M.F. Sheehan).

http://dx.doi.org/10.1016/j.csr.2017.01.016
Received 3 November 2016; Received in revised form 20 January 2017; Accepted 23 January 2017
Available online 25 January 2017

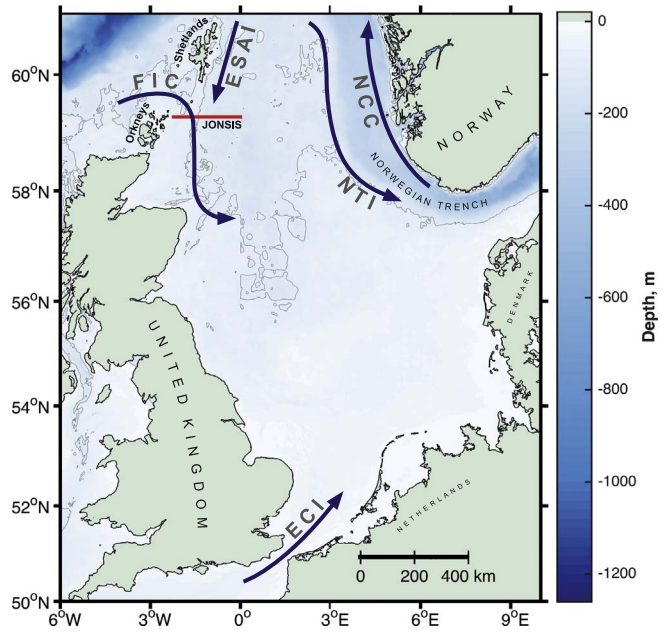

Fig. 1. Bathymetric map of the North Sea. The location of the JONSIS line and the approximate paths of the Fair Isle Current (FIC), East Shetland Atlantic Inflow (ESAI), Norwegian Trench Inflow (NTI), Norwegian Coastal Current (NCC) and English Channel Inflow (ECI) are shown (Otto et al., 1990; Turrell, 1992). Shading indicates depth from 0 to 1250 m; the 100 m isobath is marked in grey. Bathymetric data are from the GEBCO_08 grid, version 20100927 (www.gebco.net).

(Dickson et al., 1988; Holliday and Reid, 2001; Edwards et al., 2002). Reliable models of contaminant pathways and of water quality depend on accurate knowledge of these inflows (Taylor, 1987; Turrell and Henderson, 1990); reliable models of phytoplankton and nutrient distributions depend on proper physical modelling (Skogen and Moll, 2005). In the last decade, the EU's Marine Strategy Framework Directive has placed on EU member states the responsibility of ensuring "good environmental status" (EU, 2008) for their territorial waters, so providing a regional regulatory driver to efforts to improve our understanding of the physical and ecological dynamics of the North Sea.

The FIC has been described in broad terms as a southward-flowing current, approximately 30 nautical miles (56 km) wide (Svendsen et al., 1991), that flows through the Fair Isle Gap between the Orkney and Shetland islands (Dooley, 1974). In the North Sea, it is found close to the eastern coast of the Orkneys (Svendsen et al., 1991) in the approximate region of the 100 m isobath (Dooley, 1974; Winther and Johannessen, 2006). The ESAI is a more recent discovery than the FIC. In his review of the circulation of the northern North Sea, Dooley (1974) did not find evidence of a persistent inflow to the east of the Shetlands, but studies since then have found evidence of such a flow (Turrell, 1992; Turrell et al., 1996). Winther and Johannessen (2006) note that the ESAI is a more diffuse flow than the FIC, but that average transports in the two currents are similar. Between 57.5 and 58°N, the combined inflow turns east and flows towards the Norwegian coast in what has become known as the Dooley Current (Dooley, 1974; Otto et al., 1990; Winther and Johannessen, 2006). Little water from northwestern inflows reaches the southern North Sea (Pohlmann and Puls, 1994).

Previous studies in the region (e.g. Turrell, 1992) have separated the Atlantic inflow into wind-driven and non-wind-driven components, and have assumed that the wind-driven component represents the depth-constant flow that remains once the bottom-referenced geostrophic shear has been removed from the velocity profile. Subsequent references to wind- and non-wind-driven flow follow this convention.

The Atlantic inflow exhibits seasonal variations (Dooley, 1983; Turrell, 1992). It is thought to be primarily non-wind-driven in summer and primarily wind-driven in winter (Dooley, 1983; Otto et al., 1990; Svendsen et al., 1991; Turrell, 1992; Pohlmann and Puls, 1994; Winther and Johannessen, 2006). During the spring, stratification develops offshore of both the Orkney and Shetland archipelagoes as atmospheric heating warms the surface, isolating cool, dense waters left over from the previous winter beneath the thermocline (Svendsen et al., 1991; Turrell, 1992; Turrell et al., 1996; Hill et al., 2008). Closer to the shore, tidal currents are sufficiently strong that the water column remains fully mixed even when deeper, offshore waters are stratified (Svendsen et al., 1991). The density front that emerges between these two regions drives an along-front jet between the dense bottom water in the offshore, stratified region and the lighter water in the coastal mixed region (Svendsen et al., 1991; Turrell, 1992; Hill et al., 2008). This density pattern is common on the northwestern European shelf and makes the FIC and ESAI part of the thermohaline circulation that is a common feature on the northwestern European continental shelf in summer (Brown et al., 1999; Hill et al., 2008). The zonal salinity distribution reinforces this density pattern. The waters of the FIC originate along the western coast of Scotland where, prior to entering the North Sea, they are mixed with fresh water of terrestrial origin (Turrell et al., 1990; Turrell, 1992). The salinity gradient between water that exhibits this fresh water influence and more saline water found offshore may be traced around the northern coast of Scotland (Dooley, 1974). The lack of major river systems on, and the relatively small landmass of, the Orkney and Shetland Islands, means that further appreciable addition of fresh water to the FIC and ESAI from terrestrial sources does not occur in the vicinity of these archipelagoes.

The switch to a wind-driven regime occurs because wind forcing is stronger in winter (Coelingh et al., 1996; Siegismund and Schrum, 2001). Winds from the west and north tend to force an anti-clockwise circulation around the northern North Sea, a pattern that promotes inflow of water from the northwest (Furnes, 1980). The correlation between volume transport in the inflows and the North Atlantic Oscillation (NAO; Hurrell et al., 2003), an index which characterises the meridional pressure difference across the North Atlantic and the strength of westerly winds in the region, is higher at this time of year than it is in summer (Winther and Johannessen, 2006; Hjøllo et al., 2009). The breakdown of thermal stratification is also important (Turrell et al., 1990): the disappearance of the thermocline enhances Ekman transport throughout the water column (Winther and Johannessen, 2006) and reduces the density difference between near- and offshore regions, lessening the influence of the horizontal density gradient on the circulation (Turrell, 1992). A horizontal salinity gradient persists between the low-salinity coastal water and the high-salinity water of Atlantic origin towards the centre of the North Sea (Turrell, 1992), but Prandle (1984) estimates that it drives a flow an order of magnitude less than that driven by the wind.

Our understanding of the annual cycle of non-wind-driven flow in the Atlantic inflow has, to date, been based on observations from limited periods of time. Previous studies have relied on current meter records from a few months and on hydrographic observations from single cruises (e.g. Furnes, 1980; Turrell et al., 1990; Brown et al., 1999). Descriptions of the hydrography and flow in the region based on long-term observations are lacking in the literature. Volume fluxes are known to be limited by narrow sampling windows when estimated from observations (Hjøllo et al., 2009), and the role of non-wind-driven forcing in winter is not well understood (Dooley, 1983). Furthermore, the effect of horizontal temperature and salinity gradients on the non-wind-driven flow is yet to be considered separately. That stratification and horizontal temperature gradients influence the current has been understood for some time (Backhaus and Maier-Reimer, 1983; Turrell, 1992), as has the role of thermohaline circulation in the shelf seas more generally (Hill et al., 2008). The influence of horizontal salinity gradients on the Atlantic inflow has received less attention, and no attempt has been made to describe and quantify the separate influence of temperature and salinity gradients.

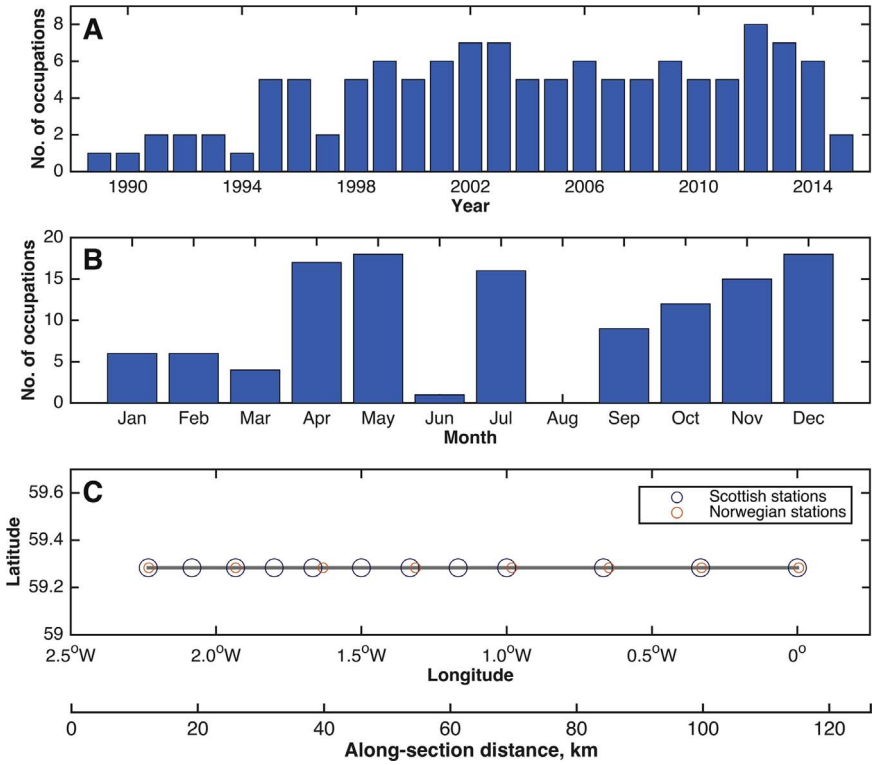

Fig. 2. Occupations of the JONSIS line: **A** by year and **B** by month. **C** Scottish and Norwegian stations on the JONSIS line.

This study analyses 27 years of data from a hydrographic section in the northern North Sea. The annual cycle of non-wind-driven forcing of, and transport in, the Atlantic inflow is quantified from this newly compiled data set, and the separate roles played by temperature and salinity on the non-wind-driven forcing are investigated.

2. Methods

The Joint North Sea Information System (JONSIS) line is a zonal section between 0°and 2.233°W at 59.28°N (Fig. 1). The section is occupied multiple times a year (Fig. 2) by Scottish research ships, which sample at 12 stations, and Norwegian research ships, which occupy a section at the same latitude known as the Orkney-Utsire line that crosses the entire North Sea; 8 stations on the Orkney-Utsire line fall between 0°and 2.233°W (Fig. 2). Temperature and salinity profiles from Scottish occupations were obtained from Marine Scotland's data archive; temperature and salinity profiles from Norwegian occupations were obtained from the online data portal of the International Council for the Exploration of the Sea (ICES) (www.ocean.ices.dk/HydChem). Scottish and Norwegian data were visually inspected to identify complete sections; isolated data points, sections with fewer than eight stations, sections with unevenly spaced stations, and sections with poor vertical resolution (i.e. profiles with measurements at greater than 1 m intervals, the standard being 1 m resolution) were rejected. The combined Scottish-Norwegian dataset comprises 122 sections, between December 1989 and April 2015 (Fig. 2). Data are available for every month apart from August; a limited number of sections are available for January, February and March, and only one section is available for June (Fig. 2). In situ temperature and practical salinity were converted into conservative temperature and absolute salinity respectively (IOC et al., 2010); all subsequent uses of temperature and salinity refer to these TEOS-10 variables. This definition of salinity gives values that are typically 0.2 higher than those reported in previous studies that used different definitions of salinity.

An objective mapping technique (Bretherton et al., 1976; Denman and Freeland, 1985; Chereskin and Trunnell, 1996) based on a Gaussian weighting function was used to interpolate the data onto a regular grid. Grid spacing was 0.01° (567 m) in the horizontal and 2 m in the vertical. Semivariograms were used to determine appropriate correlation length scales for the mapping process. Semivariograms quantify the dissimilarity (i.e. the semivariance) between observations as a function of the distance between them (Schaeffer et al., 2015). The maximum permissible correlation length scale is the distance at which dissimilarity ceases to increase with distance, although the correlation length scale may be set below this maximum (Janssen et al., 1999). The correlation length scales were 0.3° longitude (28.4 km) and 2 m in the horizontal and vertical respectively. These values are considerably less than the maximum possible correlation length scales, reflecting the need to use only the most closely correlated neighbouring data points in the interpolation, for instance, to preserve sharp thermoclines. Larger length scales produced temperature and salinity fields that were unrealistically smooth and which did not agree well with the non-gridded observations.

After the objective mapping process, in cases where the observations did not cover the entire water column, the deepest interpolated measurement was extrapolated to the seafloor using a fixed-value method; similarly, where necessary the shallowest interpolated measurement was extrapolated to the surface using a fixed-value method. Such extrapolations were carried out over a depth range of typically no more than 5 m, and extrapolations to the surface were always within the surface mixed layer. Bathymetry was extracted from the GEBCO dataset (GEBCO_08 grid, version 20100927, www.gebco.net. An example Marine Scotland section from September 1990 showing observations and the interpolated data is presented in Fig. 3. The instrumental and gridding errors are estimated to be two to three orders of magnitude smaller than the variability discussed in Sections 3–6.

Hydrographic data are presented as seasonal (JFM, AMJ, JAS and OND) mean sections; volume transport is presented as monthly mean values. Geostrophic velocity and volume transport are calculated section by section, prior to averaging, rather than from seasonally averaged distributions of temperature and salinity. Geostrophic velo-

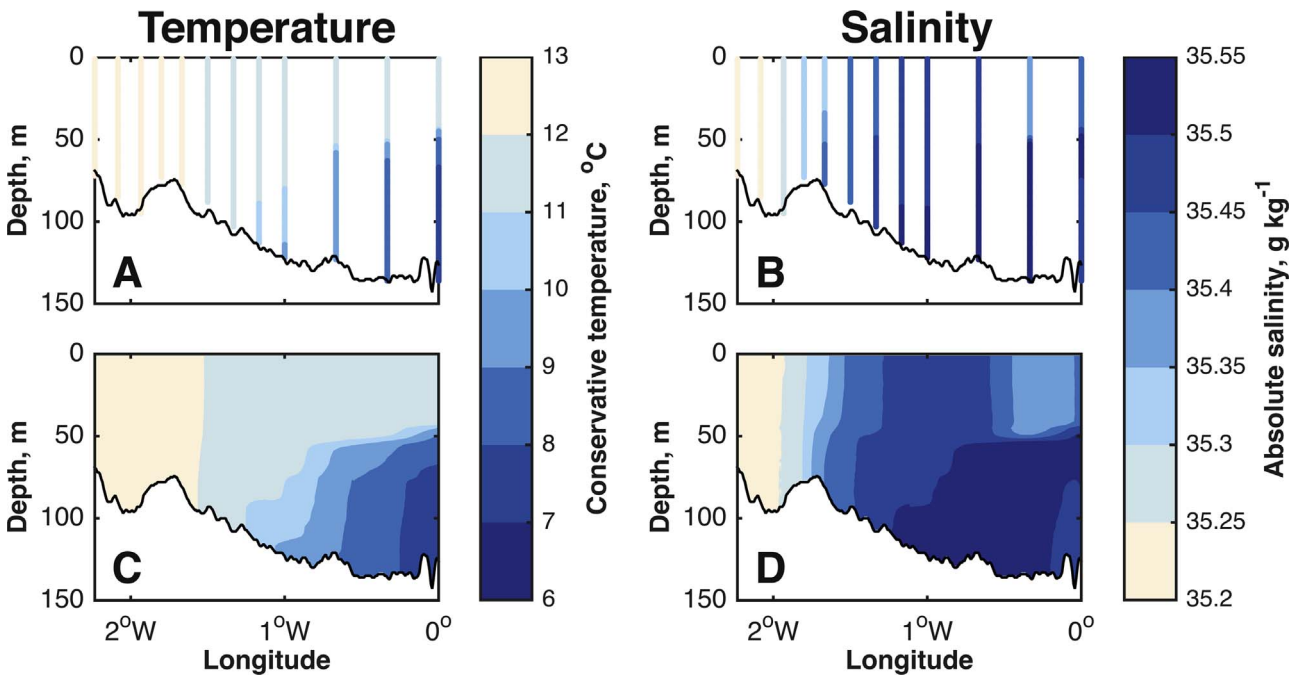

Fig. 3. A comparison of raw and interpolated data for an exemplar section **A** Observations of conservative temperature (°C) and **B** observations of absolute salinity (g kg^{-1}). **C** Optimally interpolated conservative temperature (°C) and **D** optimally interpolated absolute salinity (g kg^{-1}).

city is calculated relative to an assumed level-of-no-motion at the deepest common level between adjacent horizontal grid points. In order to assess the relative contributions that temperature and salinity make to this velocity, the components of geostrophic flow driven by the temperature and salinity distributions are also calculated. The temperature-driven component is defined as the geostrophic velocity calculated using the observed temperature distribution for a given section and an artificial salinity distribution in which salinity is constant in space. The salinity-driven component is defined as the geostrophic velocity calculated using the observed salinity distribution for a given section and an artificial temperature distribution in which temperature is constant in space. The constant salinity value is the spatial and temporal mean salinity calculated from all 122 sections (35.33 g kg^{-1}); the constant temperature value is the spatial and temporal mean temperature calculated from all 122 sections (9.05 °C). So if geostrophic velocity, v, is a function of temperature, t, salinity, S and depth, z, the temperature-driven component is $v(t, \bar{S}, z)$ and the salinity-driven component is $v(\bar{t}, S, z)$ where an overbar denotes a spatial and temporal mean.

The amplitudes and phases of the annual cycle of temperature, salinity and geostrophic velocity at each grid point are calculated using a harmonic analysis method (Thomson and Emery, 2014); the fitted (cos)sinusoids are required have a period of 365 days. This allows the construction of a sinusoidal annual cycle at each grid point for the three variables. Sampling a grid point's sinusoid at the time of each section and subtracting this value from the observed value permits the calculation of residual distributions of temperature, salinity and geostrophic velocity for each section. We will refer to these as de-seasoned distributions. Similarly, a sinusoidal annual cycle of 365 days is fitted to the time series of volume transport, and the residual (de-seasoned) time series calculated. The de-seasoned variables, once spatially averaged by section, are used to calculate the one-dimensional time series of section-mean temperature, section-mean salinity and section-integrated volume transport discussed in Section 6. Long-term trends were not removed from the data. The NAO index used in Section 6 was downloaded from NOAA's Climate Prediction Centre (www.cpc.ncep.noaa.gov/products/precip/CWlink/pna/nao.shtml), and the Atlantic Multidecadal Oscillation (AMO) index, which characterises the interdecadal variability of sea-surface temperature in the Atlantic once the signal of anthropogenic climate change has been removed (Schlesinger and Ramankutty, 1994; Trenberth and Shea, 2006), was downloaded from NOAA's Earth System Research Laboratory (www.esrl.noaa.gov/psd/data/timeseries/AMO; un-smoothed product).

3. Mean conditions over an annual cycle

3.1. Winter

In winter, there is very little spatial variation in temperature, either horizontally or vertically (Fig. 4A). Consequently, the temperature-driven component of the geostrophic flow is small: current speeds peak at approximately 1 cm s^{-1} flowing northward in the far west of the section. The horizontal salinity gradient is strong (Fig. 4B). Salinity increases from less than 35 g kg^{-1} at the western limit of the section to over 35.4 g kg^{-1} at the eastern limit. The strongest salinity gradient, the boundary between low-salinity coastal water and high-salinity water of Atlantic origin (Dooley, 1974; Turrell et al., 1990), is found west of 1.5°W. This salinity gradient drives a salinity-dependent geostrophic flow approximately 60 km wide with peak southward current speeds of over 4 cm s^{-1}. The salinity-driven flow is at its strongest in March, when southward current speeds exceed 7 cm s^{-1} at the surface. This is caused by a strengthening of the horizontal salinity gradient between 1.5 and 2°W.

The signal of the salinity-driven component is clearly visible in the depth-varying geostrophic flow (Fig. 4C). The weak temperature-driven component has little impact, despite flowing in the opposite direction. The identification of a marked horizontal salinity gradient across the JONSIS line in winter, particularly in March, and the attribution to this gradient of a defined depth-varying southward current, provides evidence of the winter-time non-wind-driven component of the Atlantic inflow proposed by Dooley (1983) but thought non-existent by Turrell (1992). However, contrary to the suggestion of Dooley (1983), this component is a narrow, near-coast feature, rather than being spread over too wide an area to be readily observed.

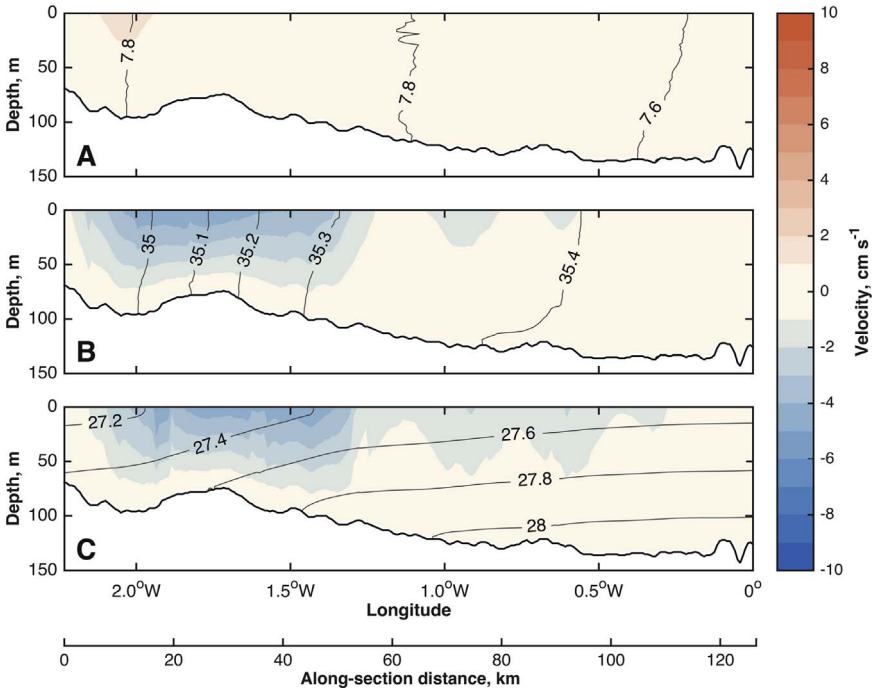

Fig. 4. Mean conditions in January, February and March. **A** Geostrophic velocity calculated using an assumed uniform salinity of 35.33 g kg^{-1} (shading; cm s^{-1}); conservative temperature (contours; °C). **B** Geostrophic velocity calculated using an assumed uniform temperature of 9.05 °C (shading; cm s^{-1}); absolute salinity (contours; g kg^{-1}). **C** Geostrophic velocity (shading; cm s^{-1}); density (contours; kg m^{-3}). Negative velocity indicates southward flow.

The mean surface geostrophic currents are slower than those predicted by models when the influence of the wind is taken into account. Winther and Johannessen (2006), in a modelling study that includes wind-driven flow, find surface currents across the western part of the JONSIS line to be approximately 20 cm s^{-1} in February; in the east, current speeds are approximately 6 cm s^{-1}. That such current speeds are not observed in the present study when wind forcing is not taken into account is consistent with the dominant role played by the wind in driving Atlantic inflow in winter.

3.2. Spring

In spring, thermal stratification begins to develop in the eastern half of the JONSIS line (Fig. 5A). The lack of stratification west of 1.5°W is evidence of the near-shore tidal mixing identified by Svendsen et al. (1991). The weak horizontal temperature gradient between the stratified and mixed regimes induces a weak, southward, temperature-driven component of the geostrophic flow, with maximum speeds of only 1 cm s^{-1}. This temperature-driven flow strength-

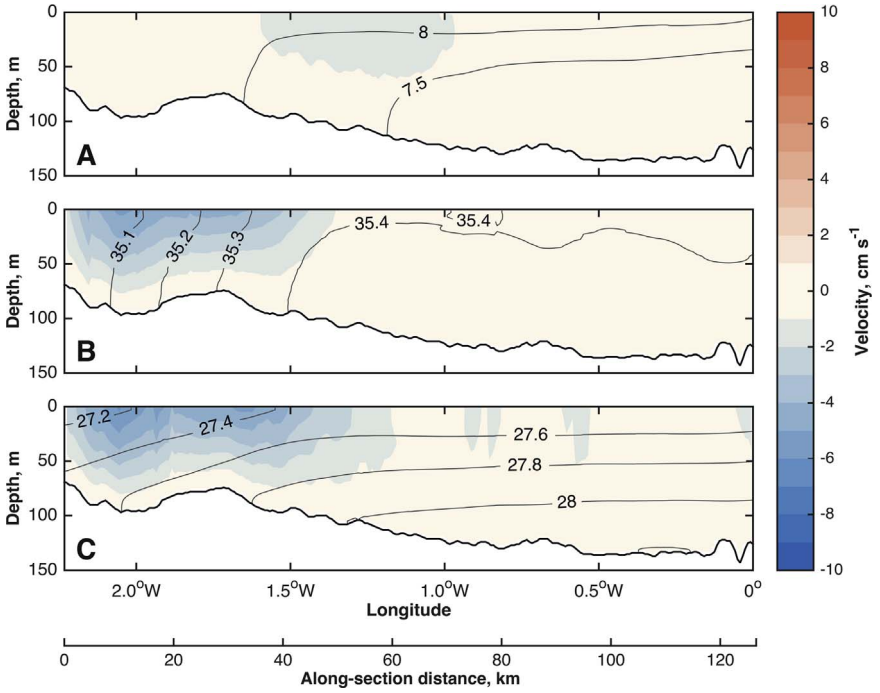

Fig. 5. Mean conditions in April, May and June. Panels, shading, contours and units are as in Fig. 4.

ens as spring progresses. There is only one section available in June (Fig. 2), but this section has a temperature-driven flow faster (4 cm s^{-1}) and wider (50 km) than the average presented here. Mean salinity in the far west of the section is higher than in winter, and a slight surface freshening leads to the development of a weak halocline east of 1.5°W (Fig. 5B). The increase in salinity in the west of the section is balanced by the westward expansion of high-salinity water, as demonstrated by the westward displacement of the 35.4 g kg^{-1} isohaline, rather than by a commensurate salinity increase in the east. This contradicts previous studies which found that the horizontal salinity gradient was kept constant by equal changes in the salinity across the FIC, rather than to changes to the extent of high- and low-salinity waters (Turrell, 1992). The salinity-driven component of the geostrophic flow remains of a comparable speed to that in winter, but is narrower (approximately 40 km wide) and centred further east. In the June section, the salinity-driven flow is much weaker than this average, being 30 km wide and having a maximum speed of 2 cm s^{-1}.

The geostrophic flow observed in spring (Fig. 5C) is present as two separate cores with peak southward velocities of over 5 cm s^{-1}, one centred at 2.1°W and the other at 1.6°W. The western core is driven by the salinity component. The eastern core is driven primarily by the salinity component, but with a contribution from the temperature component. An individual section may exhibit either one or both of the cores visible in the long-term mean. The temperature component appears to be responsible for the region of low velocity (<2 cm s^{-1}) flow that extends to the east of the eastern core. The results for spring are in better agreement than those for winter with the model results of Winther and Johannessen (2006). In June, in the west of the section, they report surface speeds of approximately 10 cm s^{-1}, and in the east report surface speeds of below 4 cm s^{-1}. This suggests that, as stratification develops, the non-wind-driven flow accounts for a greater proportion of total flow than it did in winter, both as the wind-driven component of the flow has weakened and the non-wind-driven component has strengthened.

3.3. Summer

Thermal stratification reaches its peak over the summer, as surface temperatures in an average year exceed 13 °C (Fig. 6A). Tidal stirring west of 1.5°W mixes heat throughout the water column: bottom temperatures in the mixed region are approximately 4 °C higher than bottom temperatures in the stratified region. Temperature-driven flow is present across almost the entire width of the section, but principally in a central core between 1 and 1.5°W with speeds in excess of 5 cm s^{-1}. As the summer progresses, temperature-driven current speeds in this central core increase as those to the west decrease. The freshening of surface waters in the east of the section has continued since the spring (Fig. 6B). This is likely evidence of incursions of low-salinity water from the NCC, transported westward across the northern North Sea via Ekman transport driven by northerly winds in summer (Sætre et al., 1988). Turrell et al. (1992) find evidence of this water in September 1987 in the centre of the northern North Sea. The salinity-driven component of the geostrophic flow remains confined to the western limit of the section. The speed of the salinity-driven flow reaches a maximum of 5 cm s^{-1} at 2.1°W, although in September this flow is broader (70 km) and considerably slower (3 cm s^{-1}) and than the average presented here. Together, the temperature and salinity stratification east of 1.5°W give rise to strong density stratification (Fig. 6C).

Depth-varying geostrophic flow is at its fastest (7 cm s^{-1}) in summer (Fig. 6C). The contributions of both the temperature- and salinity-driven components can be seen clearly. The central core of the flow, centred between 1 and 1.5°W, is driven by the temperature component, as is the weaker eastern core (0.6°W). The western core, centred at 2.6°W, is driven by the salinity component, but is amplified by the weak (2 cm s^{-1}) temperature component that is also found in that region.

The strongly stratified regime that these results confirm explains the different response of the Atlantic inflow to wind forcing in summer compared with winter. The effects of wind forcing take longer to be felt in summer (15–20 h) than in winter (0 h; Turrell et al., 1992). At a time when the FIC is driven primarily by the horizontal density

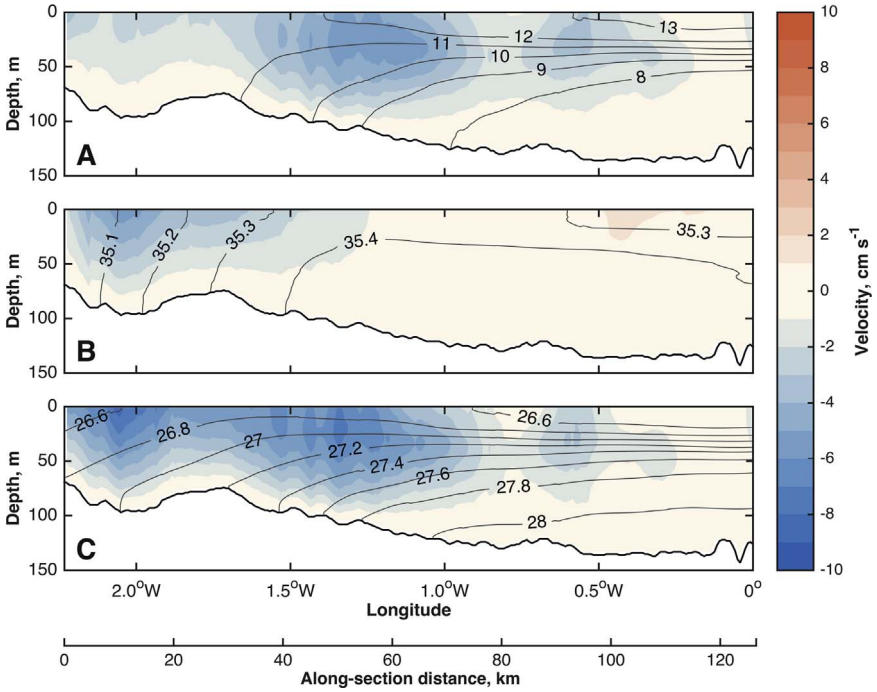

Fig. 6. Mean conditions in July and September (there is no data for August). Panels, shading, contours and units are as in Fig. 4.

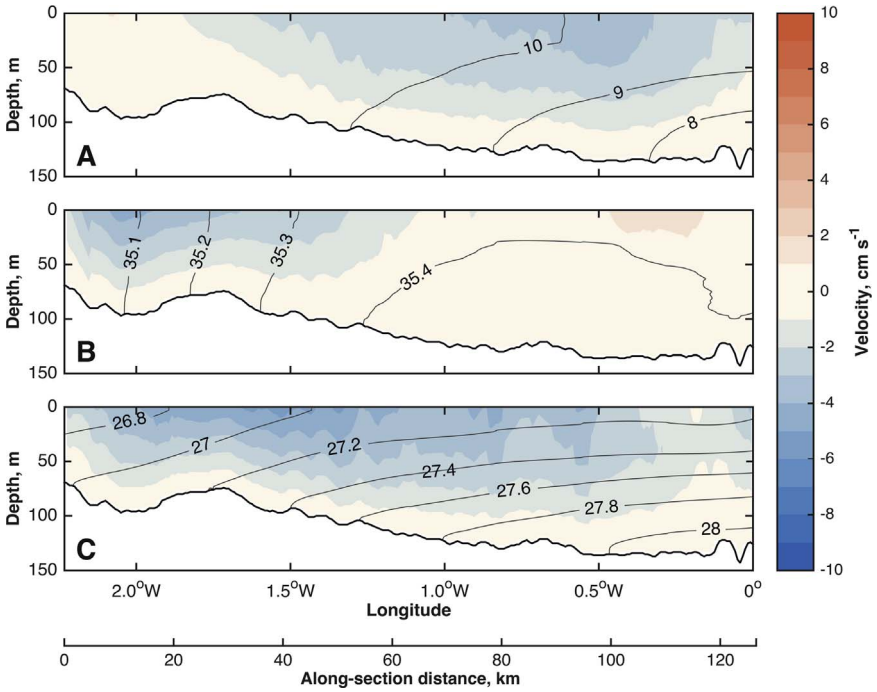

Fig. 7. Mean conditions in October, November and December. Panels, shading, contours and units are as in Fig. 4.

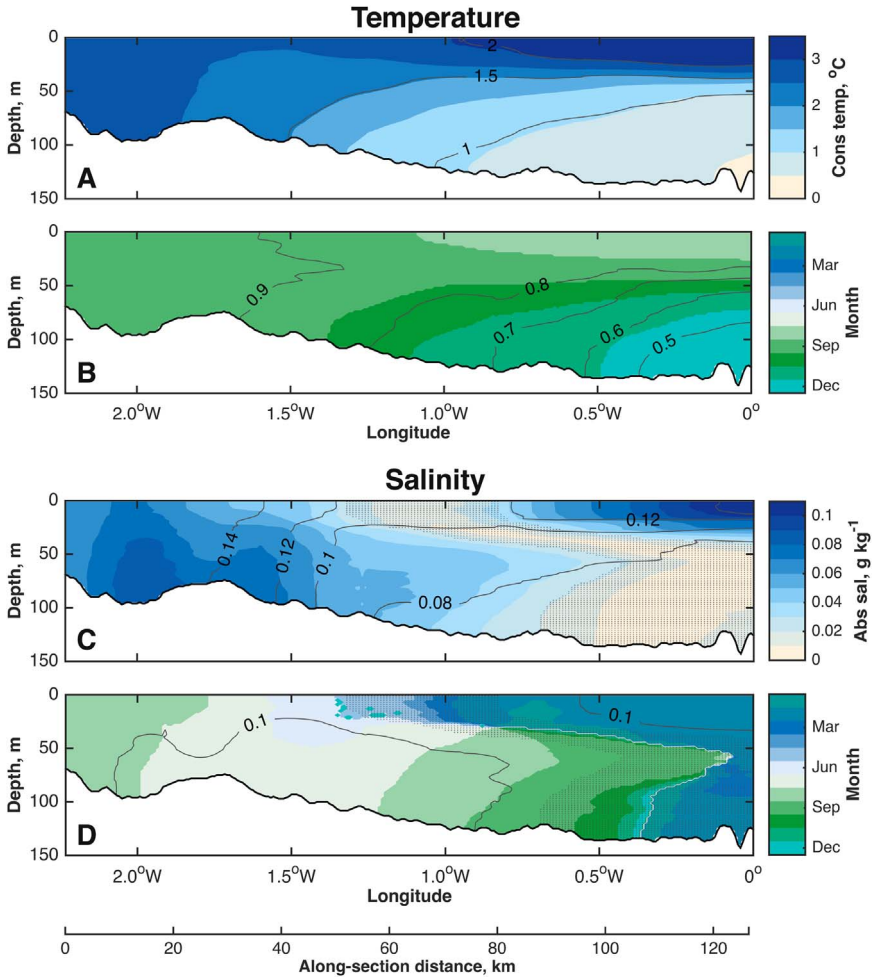

Fig. 8. A Amplitude of the annual cycle of conservative temperature (shading; °C) and standard deviation of conservative temperature (contours; °C). **B** Phase of the annual cycle as month of maximum temperature (shading) and goodness of fit of the annual cycle (R^2; contours). **C** and **D** As A and B but for absolute salinity (g kg^{-1}). Grey dots cover regions where the annual cycle does not provide a statistically significant fit to the observations at the 5% significance level (i.e. $p > 0.05$).

gradient (Turrell, 1992), and when stratification inhibits a barotropic response to wind forcing, it is the horizontal density gradient (Fig. 6C) that must adjust to changes in the overlying wind stress. Turrell et al. (1992) propose that northerly winds promote the inflow of high-salinity Atlantic water that, at the JONSIS line, sits beneath the thermocline (Fig. 6B). In turn, this strengthens the horizontal salinity gradient and so increases geostrophic flow. Conversely, they propose that southwesterly winds reduce the inflow of high-salinity Atlantic water and so weaken the horizontal salinity gradient (Turrell et al., 1992). Winther and Johannessen (2006) find that northerly winds lead to upwelling of approximately 0.5 m day^{-1} around the coast of the Shetland Islands, increasing northwards towards the shelf break. This, too, could bring high-salinity water of Atlantic origin into the northern North Sea.

3.4. Autumn

Temperature stratification and salinity stratification weaken in the autumn (Fig. 7A and B). The horizontal gradients also weaken substantially, with a corresponding weakening of the temperature- and salinity-driven components of the geostrophic flow. Maximum temperature-driven speeds are 3 cm s^{-1}; maximum salinity-driven speeds are 4 cm s^{-1}. A reversal of the horizontal salinity gradient between 0.2 and 0.5°W induces a weak (1 cm s^{-1}) northward flow at the same location. Month to month, as autumn progresses, the core of the temperature-driven flow moves eastward as the location of the horizontal temperature gradient moves offshore. The location of the salinity-driven flow remains largely unchanged. The maximum speed of the geostrophic flow is 5 cm s^{-1}, but the flow is at its broadest (approximately 110 km) in autumn. The western part of the flow is driven by the salinity component; the eastern part of the flow is driven by the temperature component. The region of weaker flow at 0.2°W appears to be a result of the northward salinity-driven flow mentioned above.

Results from the Autumn Circulation Experiment suggest that wind forcing switches from the summer, non-wind-driven regime to the winter, wind-driven regime in November and December (Turrell et al., 1990). By December, once stratification has decayed almost completely, greatest inflow is induced by southwesterly winds (Turrell et al., 1990). This suggests that a barotropic response to wind forcing is once again dominant by the end of autumn.

4. Amplitude and phase of the annual cycle

High amplitudes (>2 °C) of the annual cycle of temperature (Fig. 8A) are found in regions that are subject to the greatest degree of warming in the summer: the well-mixed coastal region and the surface in the stratified region. These same regions have higher R^2 values (>0.8; Fig. 8B), indicating that the annual cycle explains a greater portion of the observed variability in these regions than it does elsewhere, i.e. in the sub-thermocline region of Atlantic water. Maximum temperatures at the surface and in the mixed regions are reached in August and September (Fig. 8B). In the stratified region, maximum temperatures are reached progressively later with depth. At the seabed, east of 0.5°W, maximum temperature is not reached until December once stratification has broken down. In this region of Atlantic influence, where annual variability is lowest, the correlation between the derived annual cycle and the observations is at a minimum, indicating that processes other than the annual cycle of air temperature and insolation have a greater impact on the annual cycle of temperature here than they do elsewhere in the section. The annual cycle of temperature provides a statistically significant fit to the observations at all longitudes and depths of the JONSIS line. The strength of this fit is also reflected in the high degree of qualitative similarity between the distribution of the standard deviation of temperature and of the amplitude of the annual cycle of temperature (Fig. 8).

The amplitude of the annual cycle of salinity is highest (>0.1 g kg^{-1}) at the surface east of 0.2°W (Fig. 8C) in the region that is most influenced by incursions of NCC water in the summer (Fig. 6; Sætre et al., 1988). Amplitude is also high (>0.08 g kg^{-1}) at the seafloor around 2°W. This reflects the changing strength of the horizontal salinity gradient between coastal and Atlantic waters (Dooley, 1974) that occurs over an annual cycle. A horizontal gradient in standard deviation separates the relatively high-amplitude, high-variability region to the west from the region at depth to the east where salinity is less variable. That contours of standard deviation cross contours of amplitude around 1.5°W indicates that there is salinity variability at the surface that is not explained by the annual cycle. Maximum salinity in the east and west of the section occurs approximately six months out of phase (Fig. 8D): in the east, it occurs in February; in the west, it occurs in July and August. These results suggests that the amplitude of the annual cycle of salinity is not the same across the JONSIS line and that changes do not happen in phase; this contradicts previous studies based on limited data (Turrell, 1992). Changes in the strength of the salinity-driven geostrophic flow from month to month, although small, occur as a result of zonal differences in the amplitude and phase of the annual cycle of salinity. However, the correlation between the annual cycle and the observations is low (Fig. 8D), indicating that the annual cycle presented here explains only a small part (around 10%) of the observed variability. The correlation is strongest in the region of NCC influence to the east of the JONSIS line, which is likely explained by the strong influence that the lateral extent of this low-salinity water is known to have on the salinity of the northeastern North Sea (Marsh et al., 2017). In regions where the annual cycle of salinity is of low amplitude, the annual cycle does not provide a statistically significant fit to the observations at the 5% significance level.

The annual cycle of geostrophic velocity has two regions of high amplitude (>2 cm s^{-1}; Fig. 9A): the first west of 2°W, and the second centred at 1.2°W. The region of low variability in between is where annual mean geostrophic velocity (not shown) is highest: this is the location of the most persistent flow over an annual cycle. Both high-amplitude regions are caused more by the annual cycle of the temperature-driven flow than by that of the salinity-driven flow, which is the less variable of the two (Fig. 9C and D). The temperature-driven flow is near negligible in winter but reaches speeds of over 5 cm s^{-1} in summer; consequently, regions where the greatest temperature-driven velocity is observed in summer are regions where the amplitude of the annual cycle of temperature-driven velocity is high. In contrast, the core of the salinity-driven flow is present throughout the year (Figs. 4–7). It is therefore the annual cycle of the temperature-driven flow that is the greater determinant of the annual cycle of the overall geostrophic flow.

The month of the velocity maximum becomes progressively later in the year with distance east along the JONSIS line (Fig. 9B). West of 1.6°W, maximum velocity is reached in July when the temperature- and salinity-driven components combine to produce a fast (8 cm s^{-1}) flow. As temperature takes over as the principal driver of the geostrophic flow later in the year, the month of the velocity maximum shifts gradually eastwards as the location of the horizontal temperature gradient moves eastwards. In parts of the eastern limit of the section, maximum velocity does not occur until December. The annual cycle of geostrophic velocity and of the temperature- and salinity-driven components of geostrophic velocity provides a statistically significant fit to the observations in all but small parts of the JONSIS line (Fig. 9).

5. Transport of the Atlantic inflow

Volume transport calculated from the bottom-referenced geostrophic shear across the JONSIS line (Fig. 10) is lowest in February (0.11 Sv) and highest in October (0.36 Sv). Surface velocity is highest in September, peaking at over 9 cm s^{-1}; in October, maximum velocity

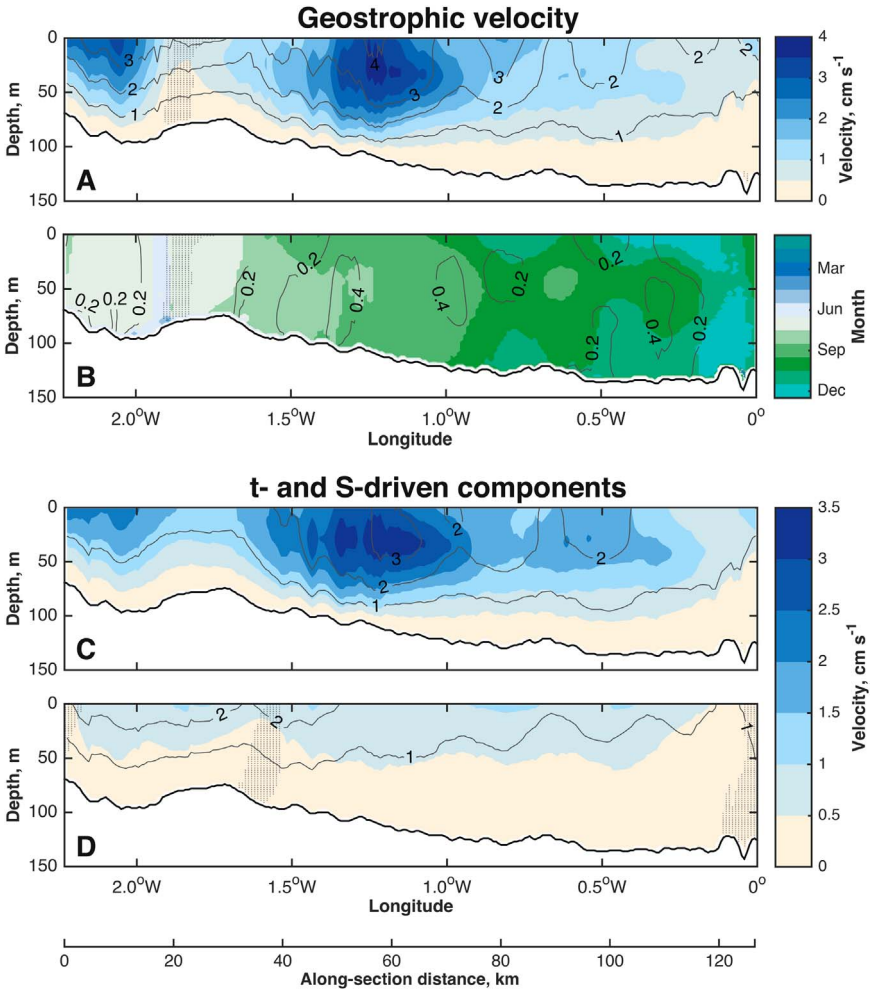

Fig. 9. Amplitude of the annual cycle of geostrophic velocity (shading; cm s^{-1}) and standard deviation of geostrophic velocity (contours; cm s^{-1}). **B** Phase of the annual cycle as month of maximum southward velocity (shading) and goodness of fit of the annual cycle (R^2; contours). **C** Amplitude of the annual cycle of temperature-driven geostrophic velocity (shading; cm s^{-1}), and standard deviation of temperature-driven geostrophic velocity (contours; cm s^{-1}). **D** As for C, but for the annual cycle of salinity-driven geostrophic velocity. Grey dots cover regions where the annual cycle does not provide a statistically significant fit to the observations at the 5% significance level (i.e. $p > 0.05$).

is lower (7 cm s^{-1}) than in September, but the flow is broader, offsetting the decline in velocity. The same is true of the temperature-driven transport: velocity peaks in September, but the broader current in October results in a higher temperature-driven transport. Maximum salinity-driven transport (0.14 Sv) occurs in January, when the salinity-driven flow is broad (approximately 90 km wide) and has a peak speed of approximately 5 cm s^{-1}. The salinity-driven current reaches its maximum speed in March, but the narrowing of the salinity-driven current between January and March offsets the increase in transport that the increase in velocity would otherwise cause.

The derived annual cycles of transport, of temperature-driven transport and of salinity-driven transport are also presented in Fig. 10. (Note that the derived annual cycles are calculated from the complete time series and not from the monthly means plotted in Fig. 10.) The derived annual cycle of transport explains 71.3% of variability in transport; the derived annual cycle of temperature-driven transport explains 86.0% of variability in the temperature-driven transport; and the derived annual cycle of salinity-driven transport explains 22.5% of variability in salinity-driven transport. The comparatively little variability in salinity-driven transport that is explained by its derived annual cycle suggests that, unlike the temperature-driven transport, the salinity-driven transport and the salinity distribution that drives it are not principally controlled by seasonally varying processes. All three derived annual cycles provide a statistically significant fit to the observations at the 1% level (i.e. $p < 0.01$). However, some features of the monthly mean transports are not accurately represented by the derived annual cycles. The derived cycles greatly underestimate transport and temperature-driven transport in March, the derived cycles being more than one standard deviation away from the respective monthly mean value in both cases. In the case of temperature-driven transport, the derived annual cycle predicts a positive (i.e. northward) transport between February and April, which is unrealistic given the monthly mean values. The addition of higher harmonics, for instance, the addition of a semi-annual cycle, was not found to make an appreciable difference to the results.

The annual cycle of transport is governed primarily by the annual cycle of the temperature-driven component. The greater amplitude of the cycle of temperature-driven transport compared with that of the salinity-driven transport, as well as the low proportion of the salinity-driven transport that is explained by its annual cycle, ensures that the annual cycle of transport most closely follows that of its temperature-driven component. Salinity-driven transport, while amplifying the temperature-driven transport throughout the year, nevertheless becomes the principal driver of thermohaline flow between January and May, maintaining a thermohaline forcing of the Atlantic inflow at a time when horizontal temperature gradients are almost negligible.

The monthly mean transport results presented above are in broad agreement with those of Turrell et al. (1990), which were derived from current meters. They estimate a non-wind-driven transport of 0.3–0.4 Sv in the FIC for periods of low wind speed (<2 m s^{-1}) during

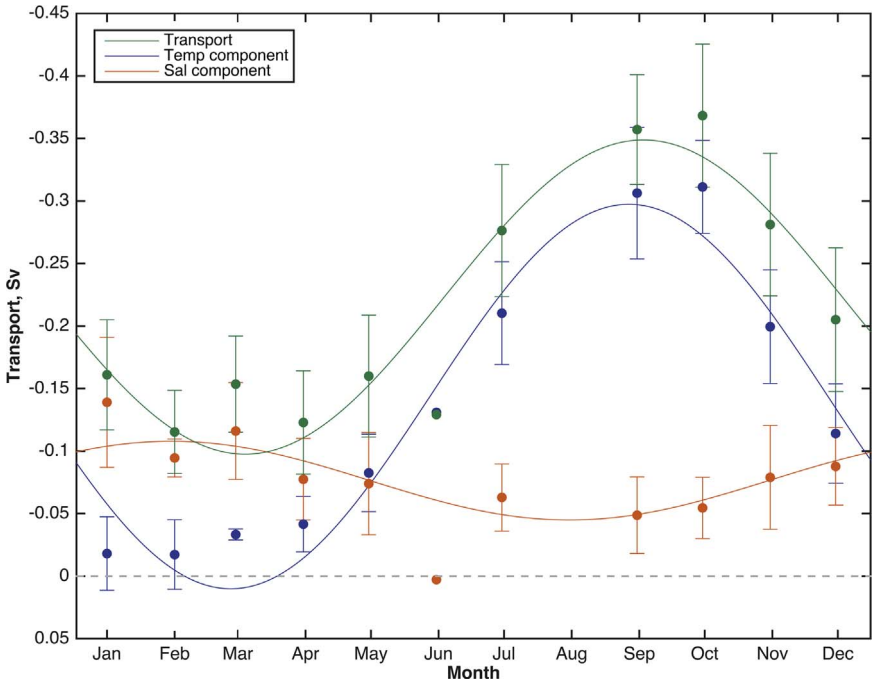

Fig. 10. Green Geostrophic volume transport across the JONSIS line over an annual cycle. **Blue** The temperature-dependent component of transport. **Orange** The salinity-dependent component of transport. Dots indicate monthly mean values, with error bars representing plus/minus one standard deviation; lines indicate the annual cycle derived from harmonic analysis. No error bars are drawn for June because only one section is available for that month. Note that the y axis has been reversed. Negative transport indicates southward flow. (For interpretation of the references to colour in this figure legend, the reader is referred to the web version of this article.)

October 1987; non-wind-driven transport reduced to 0.2–0.3 Sv in November of that year, and then to below 0.1 Sv in December. It is encouraging that estimates from current meters and hydrographic measurements yield similar results. When compared with the modelled estimates of total (i.e. wind- and non-wind-driven) transport presented by Winther and Johannessen (2006), the largest discrepancies (up to approximately 1 Sv) between non-wind-driven transport and total transport occur between December and March, a time when this study finds the former to be at a minimum and when wind-forcing is known to de dominant. In July and September, when density-forcing is dominant, the results of Winther and Johannessen (2006) suggest that wind-driven transport accounts for up to 0.1 and 0.4 Sv respectively. However, the time series presented by Damm et al. (1994) of transport through the Fair Isle Gap tends to vary between approximately 0.3 and 0.6 Sv in summer and winter respectively. Consequently, these results, together with those of the present study, imply a wind-driven transport of approximately 0.5 Sv in summer and −0.1 Sv (i.e. transport out of the North Sea) in winter. That wind forcing could drive a transport out of the North Sea in summer has been suggested by Winther and Johannessen (2006).

6. Interannual variability

Section-mean de-seasoned temperature and salinity (derived as discussed in Section 2) at the JONSIS line exhibit coherent interannual variability (Fig. 11A and B). Section-mean temperature and salinity vary in phase. They are below their respective time-series means during the 1990s; values peak in the mid-2000s before falling again towards the present day. There is no appreciable trend in de-seasoned volume transport (Fig. 11C). Interannual variability of de-seasoned salinity in the coastal waters to the west of the section is more pronounced than in the higher-salinity waters to the east of the section; however, the long-term trends in both regions are qualitatively similar to the trend calculated over the entire JONSIS line, so they are not considered separately.

Interannual variability in section-mean de-seasoned temperature and salinity is positively correlated with the AMO (Fig. 11D). Positive values of the AMO indicate anomalously warm conditions; negative values of the AMO index indicate anomalously cool conditions. With a five-year smoothing applied (i.e. the red lines in Fig. 11), variability in the AMO index explains 79.7% and 8.0% of variability in section-mean de-seasoned temperature and salinity respectively.

Interannual variability in section-mean de-seasoned temperature and salinity is negatively correlated with the NAO (Fig. 11E). The NAO is one of the key drivers of variability in the climate of the northern hemisphere (Hurrell et al., 2003) and has a strong influence on North Sea inflows (Winther and Johannessen, 2006). Only the average winter index has been considered as the NAO explains more climate variability in winter than in summer (Hurrell, 2009). With a five-year smoothing applied, variability in the NAO index explains 49.95% and 13.2% of variability in section-mean de-seasoned temperature and salinity respectively. The slopes of the regression lines associated with the temperature correlations (i.e. AMO and NAO) are significantly different from zero at the 1% significance level (i.e. $p < 0.01$). The regression lines associated with the salinity correlations are not statistically significant.

A positive AMO and a negative NAO are generally associated with a warm, salty inflow; a negative AMO and a positive NAO are generally associated with a cool, fresh inflow (Fig. 11). The link between the NAO and Atlantic inflow would likely be stronger if the wind-driven flow were included. While the NAO is thought to affect inflows to the North Sea via water mass exchange, this is secondary to the control that it exerts on the wind-driven circulation (Sündermann and Pohlmann, 2011). Marsh et al. (2017) hypothesise a strong link between Atlantic inflow into the North Sea and the salinity of the North Sea on interannual timescales. In a hindcast model simulation, they report a decline in the transport of water from the European Shelf Edge Current to the North Sea between the early 1990s and the mid-2000s, a likely consequence of the transition from a positive to a neutral NAO over the same period; in their simulation, however, this coincides with a freshening in the northern North Sea that does not appear to agree with the long-term observations presented here. Furthermore, Hjøllo et al. (2009) find that salinity in the approximate region of the JONSIS

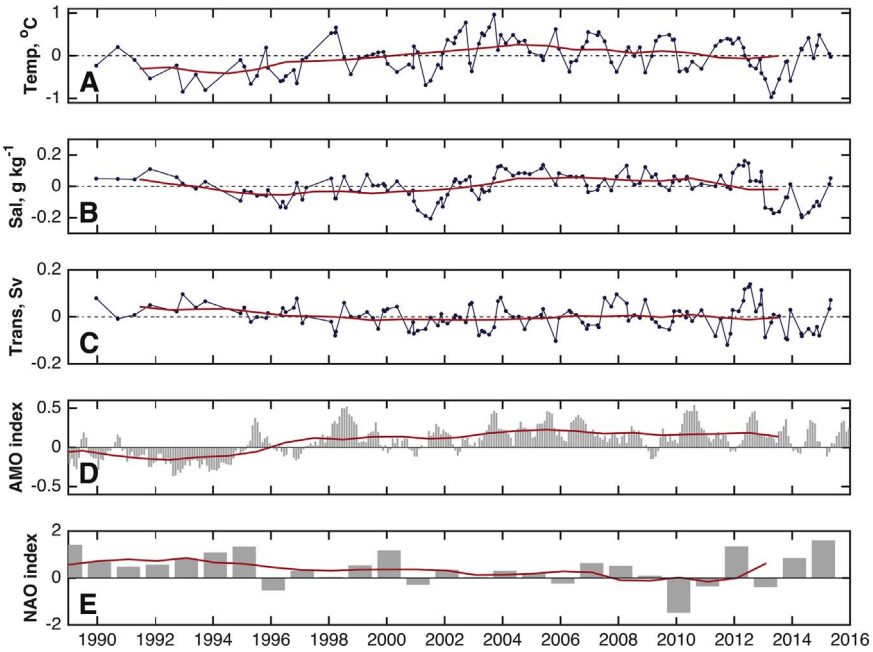

Fig. 11. Time series of section-mean de-seasoned conservative temperature (**A**; °C), absolute salinity (**B**; g kg^{-1}) and geostrophic volume transport (**C**; Sv) as an anomaly from the time-series mean (blue lines in each plot). Negative transport indicates southward flow. **D** Monthly AMO index (grey bars). **E** Mean winter NAO index (grey bars). In all panels, the red line is the five-year running mean. (For interpretation of the references to colour in this figure legend, the reader is referred to the web version of this article.)

line cannot be accurately reproduced by forcing which does not include conditions in the North Atlantic subpolar gyre; they also link a weaker circulation in the subpolar gyre to higher salinities in the northern North Sea. This suggests that the observed correlation between the NAO, AMO and mean temperature in the Atlantic inflow may be explained at least in part by large-scale variability in the circulation of the North Atlantic that occurs in response to changes in the NAO and AMO. The influence of these indices on salinity appears to be less certain, perhaps because salinity may also be affected by, for example, interannual variability in run off into the source waters of the FIC to the west of Scotland.

7. Summary

Atlantic inflow is a key control on the hydrography and ecology of the northern North Sea. Data from 27 years of occupations of the JONSIS line, a zonal hydrographic section in the northern North Sea that crosses the path of the inflow, have been analysed to describe and quantify the annual cycles of temperature, salinity and bottom-referenced geostrophic velocity. A horizontal gradient between low-salinity water near the Scottish coast and high-salinity water at depth offshore is present throughout the year. This gradient gives rise to a salinity-driven flow, the strength and location of which changes with the strength and location of the horizontal salinity gradient. The transport associated with this salinity-driven flow is stronger in winter than in summer.

There are pronounced changes in the temperature distribution over an annual cycle. Near negligible thermal gradients exist in the winter, both horizontally and vertically. In the summer a strong thermocline develops offshore in response to surface warming; however, in the shallower water close to the coast, tidal currents ensure that the water column remains fully mixed throughout the year, even when offshore waters are stratified. The growth and subsequent decay of the horizontal thermal gradient between the stratified and mixed regions give rise to a temperature-driven flow that is strongly seasonal: in the winter, very little temperature-driven flow occurs; in summer, a broad and relatively fast temperature-driven flow occurs. The transport associated with this temperature-driven flow is greater than that associated with the salinity-driven flow: the annual cycle of transport of the geostrophic shear is therefore influenced primarily by that of its temperature-driven component, being much greater in the summer than in the winter. The effect of the salinity-driven component is to maintain appreciable non-wind-driven inflow during the winter, during which season Atlantic inflow is known to be a principally wind-driven.

Section-mean de-seasoned temperature and salinity exhibit inter-annual variability, rising from anomalously low to anomalously high values between the early 1990s and the mid-2000s before declining towards the respective time-series mean value by the early 2010s. In the case of temperature, correlation with the AMO index and the anti-correlation with the NAO index are statistically significant at the 1% level.

Future work would benefit from data with higher spatial resolution in order that the often sharp vertical and horizontal gradients be better resolved. Hydrographic observations from June and August would fill in gaps in the data and would enable us to better constrain the derived annual cycles of temperature, salinity and transport during these months. Sustained observations of the wind-driven component of the flow would permit a truly comprehensive description of Atlantic inflow into the northern North Sea over an annual cycle.

These results provide a description of the density forcing of a shelf-sea current in a tidally energetic environment, accounting in detail for the influence of both temperature and salinity. The use of a 27-year-long time series allows for the calculation of robust averages and annual cycles that provide a statistically significant fit to the observations. It is hoped that these results will provide a useful background to further studies of the northern North Sea.

Author contributions

PMFS carried out the research and prepared this paper. BB, AG, RAH, KJH and SLH supported the research and provided feedback on earlier drafts of the paper.

Acknowledgements

PMFS was funded by NERC CASE Ph.D. studentship NE/L009242/1 awarded to UEA and Marine Scotland Science. PMFS thanks Bastien

Queste and Gillian Damerell for their help trouble-shooting during the data analysis. The authors gratefully acknowledge the efforts of staff and students from Marine Scotland Science (UK) and the Institute of Marine Research (Norway) with the collection of CTD data on the JONSIS and Orkney-Utsire sections from repeat hydrography programmes.

References

Backhaus, J.O., Maier-Reimer, E., 1983. On seasonal circulation patterns in the North Sea. In: Sündermann, J., Lenz, W. (Eds.), North Sea Dynamics. Springer-Verlag, Berlin, Germany.

Beaugrand, G., 2004. The North Sea regime shift: evidence, causes, mechanisms and consequences. Prog. Oceanogr. 60, 245–262.

Bretherton, F.P., Davis, R.E., Fandry, C.B., 1976. A technique for objective analysis and design of oceanographic experiments applied to mode-73. Deep-Sea Res. 23, 559–582.

Brown, J., Hill, A.E., Fernand, L., Horsburgh, K.J., 1999. Observations of a seasonal jet-like circulation at the central North Sea cold pool margin. Estuar. Coast. Shelf Sci. 48, 343–355.

Chereskin, T.K., Trunnell, M., 1996. Correlation scales, objective mapping, and absolute geostrophic flow in the California current. J. Geophys. Res. 101, 22619–22629.

Coelingh, J.P., van Wijk, A.J.M., Holtslag, A.A.M., 1996. Analysis of wind speed observations over the North Sea. J. Wind Eng. 61, 51–69.

Damm, P., Hinzpeter, H., Luthardt, H., Terzenbach, U., 1994. Seasonal and interannual variability in the atmosphere and the sea. In: Sündermann, J. (Ed.), Circulation and Comtaminant Fluxes in the North Sea. Springer-Verlag, Berlin, Germany.

Denman, K.L., Freeland, H.J., 1985. Correlation scales, objective mapping and a statistical test of geostrophy over the continental shelf. J. Mar. Res. 43, 517–539.

Dickson, R.R., Meincke, J., Malmberg, S.A., Lee, A.J., 1988. The great salinity anomaly in the northern North Atlantic 1968–1982. Prog. Oceanogr. 20, 103–151.

Dooley, H.D., 1974. Hypotheses concerning the circulation of the northern North Sea. J. du Cons. Int. Pour l'Explor. de la Mer. 36, 54–61.

Dooley, H.D., 1983. Seasonal variability in the position and strength of the Fair Isle Current. In: Sündermann, J., Lenz, W. (Eds.), North Sea Dynamics. Springer-Verlag, Berlin, Germany.

Edwards, M., Beaugrand, G., Reid, P.C., Rowden, A.A., Jones, M.B., 2002. Ocean climate anomalies and the ecology of the North Sea. Mar. Ecol. Prog. Ser. 239, 1–10.

EU, 2008. Directive 2008/56/EC of the European Parliament and of the Council, 17 June 2008 (Marine Strategy Framework Directive), Official Journal of the European Union 51(L164), 19–40.

Furnes, G.K., 1980. Wind effects in the North Sea. J. Phys. Oceanogr. 10, 978–984.

Hill, A.E., Brown, J., Fernand, L., Holt, J., Horsburgh, K.J., Proctor, R., Raine, R., Turrell, W.R., 2008. Thermohaline circulation of shallow tidal seas. Geophys. Res. Lett. 35, L11605.

Hjøllo, S.S., Skogen, M.D., Svendsen, E., 2009. Exploring the currents and heat within the North Sea using a numerical model. J. Mar. Syst. 78, 180–192.

Holliday, N.P., Reid, P.C., 2001. Is there a connection between high transport of water through the Rockall Trough and ecological changes in the North Sea? Ices J. Mar. Sci. 58, 270–274.

Hurrell, J.W., 2009. North Atlantic Oscillation. In: Steele, J., Turekian, K., Thorpe, S. (Eds.), Encyclopedia of Ocean Sciences. Academic Press, San Diego, United States of America.

Hurrell, J.W., Kushnir, Y., Ottersen, G., Visbeck, M., 2003. An overview of the North Atlantic Oscillation. In: Hurrell, J., Kushnir, Y., Ottersen, G., Visbeck, M. (Eds.), The North Atlantic Oscillation: Climatic Significance and Environmental Impact. American Geophysical Union, Washington D.C., United States of America.

IOC, SCOR, IAPSO, 2010. The international thermodynamic equation of seawater, 2010: calculation and use of thermodynamic properties (English), Intergovernmental Oceanographic Commission, manuals and guides number 56, UNESCO.

Janssen, F., Schrum, C., Backhaus, J.O., 1999. A climatological data set of temperature and salinity for the Baltic Sea and the North Sea. Germ. J. Hydrogr., Suppl. 9, 1–245.

Lindley, J.A., Roskell, J., Warner, A.J., Halliday, N.C., Hunt, H.G., John, A.W.G., Jonas, T.D., 1990. Doliolids in the German Bight in 1989: evidence for exceptional inflow into the North Sea. J. Mar. Biol. Assoc. U. K. 70, 679–682.

Marsh, R., Haigh, I.D., Cunningham, S.A., Inall, M.E., Porter, M., Moat, B.I., 2017. Large-scale forcing of the European Slope Current and associated inflows to the North Sea. Ocean Sci. (in preparation), http://dx.doi.org/10.5194/os-2016-61.

Otto, L., Zimmerman, J.T.F., Furnes, G.K., Mork, M., Sætre, R., Becker, G., 1990. Review of the physical oceanography of the North Sea. Neth. J. Sea Res. 26, 138–161.

Pohlmann, T., Puls, W., 1994. Currents and transport in water. In: Sündermann, J. (Ed.), Circulation and Comtaminant Fluxes in the North Sea. Springer-Verlag, Berlin, Germany.

Prandle, D., 1984. A modelling study of the Cs-137 in the seas of the European continental shelf. Philos. Trans. R. Soc. Lond. Ser. A 310, 407–436.

Sætre, R., Aure, J., Ljøen, R., 1988. Wind effects on the lateral extension of Norwegian Coastal Water. Cont. Shelf Res. 3, 239–253.

Schaeffer, A., Roughan, M., Jones, E., White, D., 2015. Physical and biological spatial scales of variability in the Eastern Australian Current separation zone from the shelf glider measurements. Biogeosci. Discuss. 12, 20101–20121.

Schlesinger, M.E., Ramankutty, N., 1994. An oscillation in the global climate system of 65–70 years. Nature 367, 723–726.

Siegismund, F., Schrum, C., 2001. Decadal changes in the wind forcing over the North Sea. Clim. Res. 18, 39–45.

Skogen, M.D., Moll, A., 2005. Importance of ocean circulation in ecological modeling: an example from the North Sea. J. Mar. Syst. 57, 289–300.

Sündermann, J., Pohlmann, T., 2011. A brief analysis of North Sea physics. Oceanologia 53, 663–689.

Svendsen, E., Sætre, R., Mork, M., 1991. Features of the northern North Sea circulation. Cont. Shelf Res. 5, 493–508.

Taylor, A.H., 1987. Modelling contaminants in the North Sea. Sci. Total Environ. 63, 45–67.

Thomson, R.E., Emery, W.J., 2014. Data Analysis Methods in Physical Oceanography. Elsevier Science, Amsterdam, the Netherlands.

Trenberth, K.E., Shea, D.J., 2006. Atlantic hurricanes and natural variability in 2005. Geophys. Res. Lett. 33, L12704.

Turrell, W.R., 1992. New hypotheses concerning the circulation of the northern North Sea and its relation to North Sea fish stock recruitment. Ices J. Mar. Sci. 49, 107–123.

Turrell, W.R., Henderson, E.W., 1990. Transport events within the Fair Isle Current during the Autumn Circulation Experiment. Estuar. Coast. Shelf Sci. 31, 25–44.

Turrell, W.R., Henderson, E.W., Slesser, G., 1990. Residual transport within the Fair Isle Current observed during the autumn circulation experiment (ACE). Cont. Shelf Res. 10, 521–543.

Turrell, W.R., Henderson, E.W., Slesser, G., Payne, R., Adams, R.D., 1992. Seasonal changes in the circulation of the northern North Sea. Cont. Shelf Res. 12, 257–286.

Turrell, W.R., Slesser, G., Payne, R., Adams, R.D., Gillibrand, P.A., 1996. Hydrography of the East Shetland Basin in relation to decadal North Sea variability. Ices J. Mar. Sci. 53, 899–916.

Winther, N.G., Johannessen, J.A., 2006. North Sea circulation: Atlantic inflow and its destination. J. Geophys. Res. 111, C12018.